

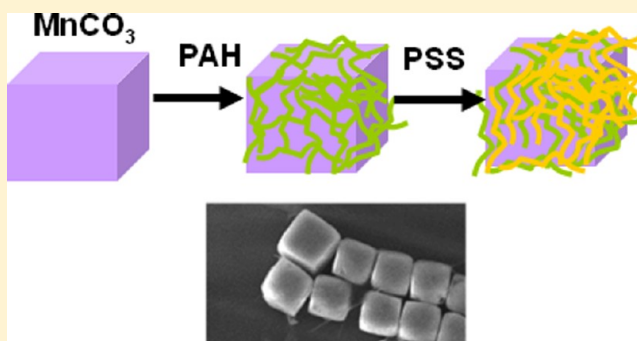
# Template-Assisted Assembly of the Functionalized Cubic and Spherical Microparticles

Milana Lisunova, Neal Holland, Olga Shchepelina, and Vladimir V. Tsukruk\*

School of Materials Science and Engineering, Georgia Institute of Technology, Atlanta, Georgia 30332, United States

## Supporting Information

**ABSTRACT:** The patterned template-assisted assembly of the cubic microparticles driven by the competing capillary, Columbic, and van der Waals forces had been studied in comparison with the traditional spherical colloidal microparticles. We observed that the spherical and cubic microparticles assembled with different probability in the channels of the hydrophobic–hydrophilic patterned substrates due to differences in a balance of adhesive and capillary forces. In contrast to highly selective assembly of spherical microparticles, selective deposition of cubic microcrystals with channels is impeded by strong adhesive forces facilitated by large specific interfacial areas between cube facets and substrate. The modification of the patterned substrate by functionalized coatings with oppositely charged topmost layers significantly increases the probability (to 86%) of the cubic microparticles to assemble into chemically modified channels. The introduction of ultrathin LbL shells on cubic microparticles and functionalization of patterned substrates are critical for the directed colloidal assembly of anisotropic microparticles into ordered aggregates.



## INTRODUCTION

Spontaneous assembly of micro- and nano-sized colloidal particles is a critically important process that plays a central role in the construction of biological structures and synthetic materials such as cells, viruses, bones, and nanocomposites.<sup>1–5</sup> The control of the particle assembly by the application of internal forces such as magnetic,<sup>6</sup> electrostatic,<sup>7</sup> and shear flow<sup>8,9</sup> could bring an additional means for the construction of the highly ordered colloidal arrays on a hierarchical mesoscale.<sup>10</sup> Understanding the principles of assembly of complex colloidal particles will point toward a novel advanced materials at which binding of the constructed blocks are governed mainly by shape geometry and anisotropic interactions which can be useful for further application in biomedical diagnostic technologies, adaptive materials, and energy conversion and conservation.<sup>11–15</sup>

The guiding assembly of colloidal microparticles on patterned substrates found to be useful approach for understanding guiding assembling principles due to its advantages in controlled deposition of the particles and for creating long-range order lattices with fewer defects (perfect colloidal crystals).<sup>16,17</sup> Such template-based assembling approaches can be used in a hierarchical fashion, where a self-assembled structure on a template itself becomes a template for the assembly of other building blocks.<sup>18</sup> For instance, Schweikart et al. organized 60 nm silica spheres into a wrinkle substrate by capillary forces upon drying on a large scale.<sup>19</sup> Kim et al. were able to control the selective deposition of the nanoparticles by a

combination of a template-assisted method as well as strong attractive electrostatic forces between the oppositely charged substrate and nanoparticles.<sup>16</sup> Apart from electrostatically driven interaction,<sup>20</sup> hydrogen-bonding-mediated assembly was applied to ligand-modified gold nanoparticles.<sup>21</sup>

The importance of the colloidal assembly into ordered arrays and its effect on the mechanical properties of column–particle nanocomposite was discussed by Hirakata et al.<sup>22</sup> The loading experiments reveal improvement of the composite material stiffness by 2-fold in comparison with those materials without nanoparticles. The positioning of the microparticles on the various templates achieved through complementary shape recognition and aided by capillary, fluidic, and gravitational forces was found to be useful for the construction field-effect transistor.<sup>23</sup> Ahniyaz et al. induced the formation of defect-free superlattices with a very high degree of orientational order by application of an external magnetic field on a dispersion of superparamagnetic nanocubes.<sup>24</sup> Patterning of nanoparticles was used to create Raman gratings and control the complex buckling patterning of ultrathin films.<sup>25,26</sup>

It is worth noting that the guided assemblies of nano- and microstructures are widely studied for spherical colloidal microparticles, while the assembly of anisotropic microparticles such as cubes has been considered only in rare cases despite the

Received: July 30, 2012

Revised: August 23, 2012

Published: August 27, 2012

fact that these microparticles are highly relevant to the design of advanced functional and biomaterials.<sup>27</sup> DeSimone et al. demonstrated that by utilizing the particle replication in nonwetting templates (PRINT) technique the parameters of anisotropic microparticles, such as shape, size, and composition, could be manipulated and assembled.<sup>28</sup> Recently, Jones et al. have synthesized one-, two-, and three-dimensional structures by using the inherent shape-directed crystallization of the DNA-mediated anisotropic nanoparticles.<sup>29</sup> Glotzer et al. determined that patchy particles can be fabricated so that arrangement of selective patches could be used to adjust the overall structures of particle assemblies.<sup>15</sup>

Moreover, usage of microscopic and submicrometer crystals with well-defined anisotropic shapes and selectively functionalized facets brings into play not only long-range weak interactions but also anisotropic steric interactions. Rycenga et al. showed the possibility to construct clusters different in size (from dimers to long chains) via functionalizing the six faces of silver cubes in different schemes that is in high contrast to the spherical isotropic colloids.<sup>30</sup> Yet another example involves assembly of tetrahedral CdTe nanocrystals into free-floating sheets via a combination of electrostatic and hydrogen-bonded interactions.<sup>31</sup> The anisotropic interactions of Janus spheres (that are hydrophobic on one hemisphere and negatively charged on the other) were shown forming a variety of complex aggregates.<sup>32</sup> Chen et al. presented the effect of the chemical anisotropy of Janus particles on the generation of highly ordered lattices.<sup>33</sup> The anisotropic interactions of the triblock Janus particles (electrostatic repulsion in the middle, hydrophobic attraction at the poles) resulted in the open Kagome lattice. The resulting lattice possesses two families of pores: one that is hydrophobic on the rims of the pores and another that is hydrophilic. Tunability of the electromagnetic properties was shown through the controlled assembly of the cubic nanoparticles within a polymer thin film.<sup>34</sup>

It is generally suggested but rarely confirmed that anisotropy of shape as well interactions results in more complex assemblies at different length scales as compared to traditional spherical colloidal microparticles. Hence, in this study, we focus on the effect of the shape on the template-assisted assembly of microparticles driven by hydrophobic–hydrophilic, capillary, and Columbic forces. Specifically, for this study we selected two types of microparticles: cubic  $\text{MnCO}_3$  microparticles and spherical  $\text{SiO}_2$  microparticles with comparable dimensions. Selection of microparticles is dictated by their uniform shape with a narrow size distribution and well-known surface chemistry appropriate for further modification. The interfacial forces were controlled by using ultrathin layer-by-layer (LbL) coatings on both patterned templates and microparticles. By modifying adsorption conditions, we easily tuned the surface potential (negative/positive) of these LbL multilayers as well as their hydrophobicity.<sup>35,36</sup> The template-assisted assembly of the cubic microparticles driven by capillary, hydrophobic/hydrophilic, and Columbic forces had been compared with that of the traditional spherical microparticles in order to reveal the role of shape on the final morphology. We demonstrated that these two types of the colloidal microparticles are assembled with very different probability in the channels of the patterned substrates due to much higher contact surface area of cubic microparticles as compared to the spherical ones that consequently results in the more pronounced role of the local tethering to the underlying substrate. The selective deposition of the cubic microparticles inside the functionalized

channels was achieved by further functionalization of their surfaces with LbL coatings.

## EXPERIMENTAL SECTION

Figure 1 depicts overall principles of the fabrication of functionalized microparticles exploited in this work. Poly(allylamine hydrochloride)

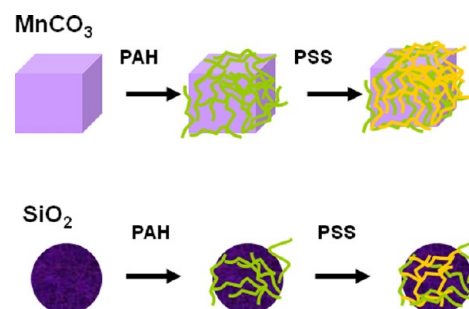


**Figure 1.** Bare and functionalized microparticles.

(PAH, molecular weight (MW) 120 kDa) was purchased from Polysciences, Inc. Polysodium 4-styrenesulfonate (PSS, MW = 70 kDa) was purchased from Sigma-Aldrich. Fluorescein isothiocyanate (FITC) was purchased from Sigma-Aldrich. Silica microparticles with diameter  $2.5 \mu\text{m}$  as 10% dispersion in water were obtained from Polysciences, Inc. Nanopure water (NANOpure Diamond water purification system, Barnstead) with a resistivity of  $18.2 \text{ M}\Omega \text{ cm}$  was used in all experiments.

Manganese carbonate crystals were prepared by mixing  $\text{MnSO}_4$  and  $\text{NH}_4\text{HCO}_3$  solutions.<sup>37</sup> First, a nanoseed solution was prepared by mixing 20 mg of  $\text{NH}_4\text{HCO}_3$  with 1 mg of  $\text{MnSO}_4$  in 100 mL of Nanopure water under rapid stirring. Then, 250 mL of 6 mM  $\text{MnSO}_4$  (with 0.5% 2-propanol) was mixed with 250 mL of 0.06 M  $\text{NH}_4\text{HCO}_3$  (with 0.5% 2-propanol) and stirred at  $80^\circ\text{C}$ . Prior to mixing, 37.5 mL of nanoseed solution was added to  $\text{MnSO}_4$  solution. The precipitate was extensively washed with Nanopure water and dried in air.

LbL assembly of  $(\text{PAH}/\text{PSS})_2$  shells has been performed according to the established procedure (Figure 1).<sup>4,38</sup> Briefly, 0.5 mg/mL of each polymer solutions was prepared by dissolving the polymers in an aqueous buffer with  $\text{pH} = 7$ . Typical deposition time on a single cycle was 15 min followed by three rinsing steps with an aqueous buffer solution ( $\text{pH} = 7$ ) to remove excess free polymer. The polymers layers were coated one after the other. After each deposition step the suspensions were centrifugated at 2000 rpm for 2 min to remove the excess polymer. Deposition, rinsing, and resuspending steps were performed on a VWR analogue vortex mixer at 4000 rpm.

A micropatterned substrate was prepared using capillary transfer lithography over a  $5 \text{ mm} \times 5 \text{ mm}$  area according to the established procedure.<sup>39</sup> A 500 nm thick polystyrene (PS) stripe pattern with a periodicity of  $10 \mu\text{m}$  (on average, regions of 4 and  $6 \mu\text{m}$ ) defined by a poly(dimethylsiloxane) (PDMS) stamp was deposited on the substrate. Three bilayers of PAH/PSS components and one more layer of PAH were deposited on a silicon substrate to create functionalized substrates according to the standard procedure used in our lab.<sup>40</sup> Spin-assisted LbL assembly was conducted with uniform coverage over the whole surface area.<sup>41,42</sup> The [100] silicon substrates (Semiconductor Processing) were cleaned with piranha solution (3:1 concentrated sulfuric acid and hydrogen peroxide mixture; *caution! piranha solution reacts violently with organic matter and should be handled with extreme care*), abundantly rinsed with Nanopure water, and dried with dry nitrogen stream in accordance with the usual procedure.<sup>43</sup>

Surface potentials of the core–shell microparticles in aqueous solutions were measured on a Zetasizer nano-ZS (Malvern). Each value of zeta-potential was obtained at ambient conditions by averaging three independent measurements of 35 runs each. Scanning electron microscopy (SEM) analysis was performed with a Hitachi S-3400-II scanning electron microscope at 10 kV. AFM imaging of

template patterns were performed on an Icon microscope with a Nanoscope V controller (Bruker) using the tapping mode and scan assist regime in air.<sup>44–46</sup> Confocal images of core–shell microparticles with FITC-labeled shells were obtained with a LSM 510 NLO META UV–vis inverted confocal laser scanning microscope equipped with 63 × 1.4 oil immersion objective lens (Zeiss). A drop of a dispersion of core–shell microparticles was added to Lab-Tek chamber (Electron Microscopy Sciences) and then filled with aqueous solution.

## RESULTS AND DISCUSSION

SEM images of the  $\text{MnCO}_3$  and  $\text{SiO}_2$  microparticles revealed the nearly monodisperse bare and coated microparticles with dimension of  $2.5 \pm 0.2 \mu\text{m}$  (Figure 2). The polymeric shells

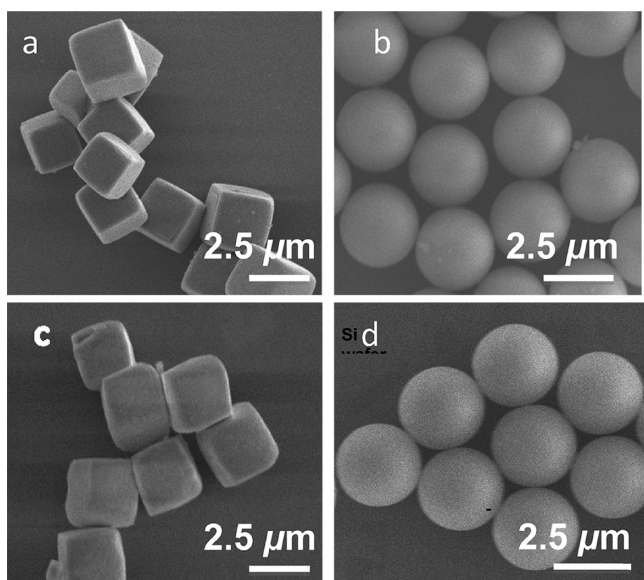


**Figure 2.** SEM images of the bare cubic  $\text{MnCO}_3$  (a) and  $\text{SiO}_2$  (b) microparticles and the same microparticles (c, d) coated with  $(\text{PAH}/\text{PSS})_2$  shells.

were assembled on the cubic and spherical cores in good agreement with our previous study on LbL assembly on  $\text{CdCO}_3$  and  $\text{CaCO}_3$  microcrystals.<sup>47</sup> Zeta-potential measurements confirm the formation of  $(\text{PAH}/\text{PSS})_2$  shells on the microparticles in aqueous dispersion with the overall negative surface potential which allows a good stability of the microparticle suspension (Table 1).<sup>48</sup> Finally, the confocal images of the dispersion of the microparticles with labeled

shells also proved the successful LbL coating on microparticles (Figure 3).

At initial state the colloidal dispersion of the microparticles was vigorously stirred to homogeneous state and drop-cast on the template substrate inclined by  $30^\circ$  from the horizontal plan and then slowly moved into the parallel direction of PS stripes (Figure 4). While the water evaporates, the receding contact

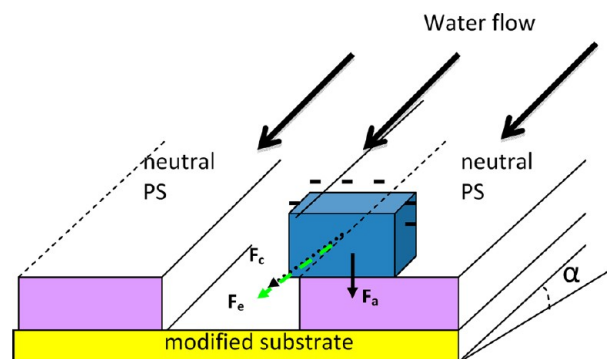


**Figure 4.** Template-assisted assembly with forces exerted on the cubic microparticles: capillary ( $F_c$ ), adhesive ( $F_a$ ), and electrostatic ( $F_e$ ) forces.

line applied a drag force on the microparticles in uniform direction. Microparticles located in the vicinity of the pinned contact line experience immersion capillary forces that might drag them into the channels. The assembling of the microparticles on the patterned substrates is a complicated process governed by many factors such as capillary forces between the substrates and the microparticles and capillary forces between the microparticles, electrostatic forces, gravitational forces, and Coulombic forces as will be discussed in detail below (Figure 4). In the current study, we focus on assembly of cubic and spherical microparticles with different negative surface charges as adsorbed to different regions of patterned substrates: hydrophobic PS regions combined with negatively charge bare silicon oxide (Figure 5a,b) or positively charged functionalized substrates (Figure 5c,d). The topography of the patterns had been chosen with respect to the shape of cubic microparticles, and their tendencies interact face to face and build linear chain structures.

First, we conducted control experiments where the bare spherical  $\text{SiO}_2$  and cubic  $\text{MnCO}_3$  microparticles were deposited on the PS patterned silicon wafer (Figure 6). In such a case,

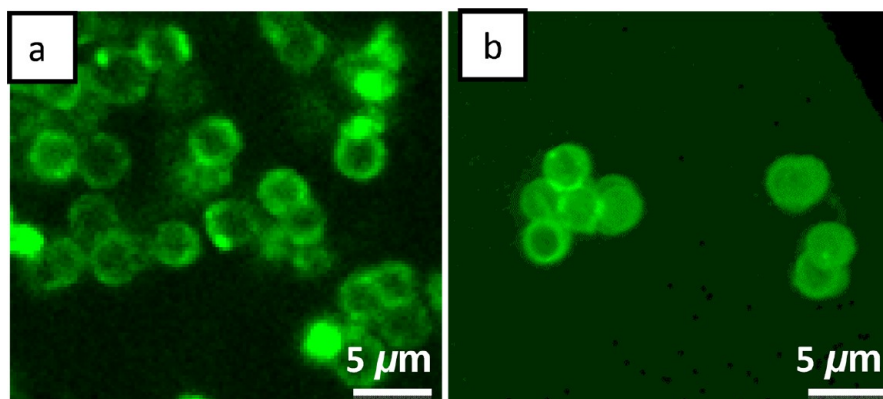


**Figure 3.** Confocal images of cubic (a) and spherical (b) microparticles with labeled shells.

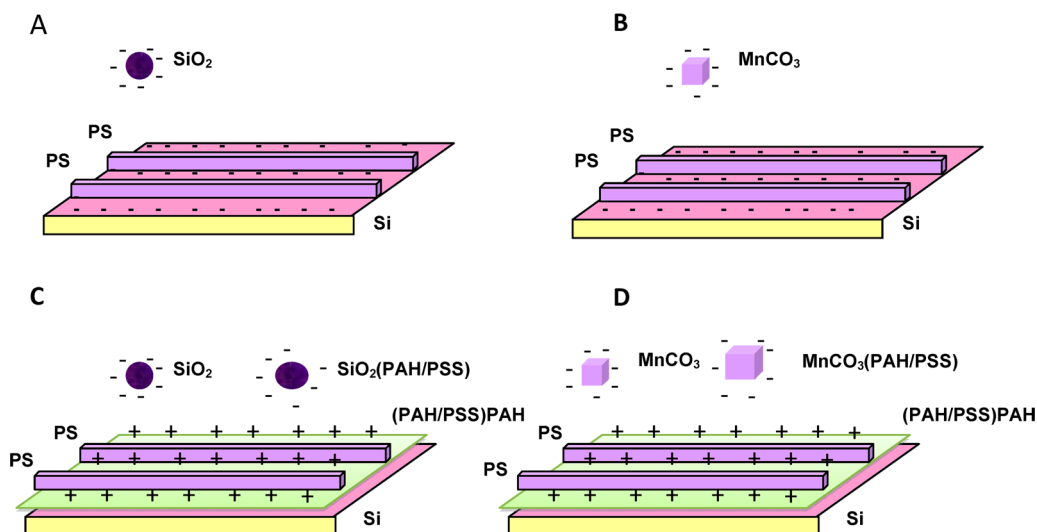


**Figure 5.** Selective assembly of cubic and spherical microparticles on patterned templates.

**Table 1. Zeta Potential Values of the Colloidal Particles and Substrates**

substrate/particle	zeta-potential (mV) at pH 7
MnCO <sub>3</sub>	-10.8 ± 1.3
MnCO <sub>3</sub> -(PAH/PSS) <sub>2</sub>	-15.4 ± 2.6
SiO <sub>2</sub>	-22.5 ± 3
SiO <sub>2</sub> -(PAH/PSS) <sub>2</sub>	-23.3 ± 7
silicon wafer (after piranha treatment)	-35 (ref 65)
silicon wafer functionalized by (PAH/PSS) <sub>3</sub> PAH	+40 ± 7

despite on the strong repulsion forces between the spherical microparticles and the silicon substrate we observe a strong tendency of the spherical microparticles to assemble mainly on the hydrophilic bare silicon substrate between the PS ridges, with probability about 95%. Apparently, the capillary forces are

strong enough to drive almost all spherical microparticles in the channels. This selective adsorption is in a high contrast to the assembly of bare cubic microparticles that localized relatively randomly on all regions of patterns disregarding local topography and composition (Figure 6). We suggested that the strong facet–surface interactions lead to the high level of cubic microparticle aggregation and their landing and strong tethering to random sites disregarding to the capillary force acts.

Thus, in order to induce the electrostatic attraction between the bare substrate and the microparticles and control the capillary forces that drive microparticles to the channels, the silicon wafer was modified by the positively charged LbL coating (surface potential changed from -35 to +40 mV (see Table 1 and Figure 5)). Under these conditions, the spherical microparticles are again selectively located on positively charged surface areas between PS regions (Figure 7). The

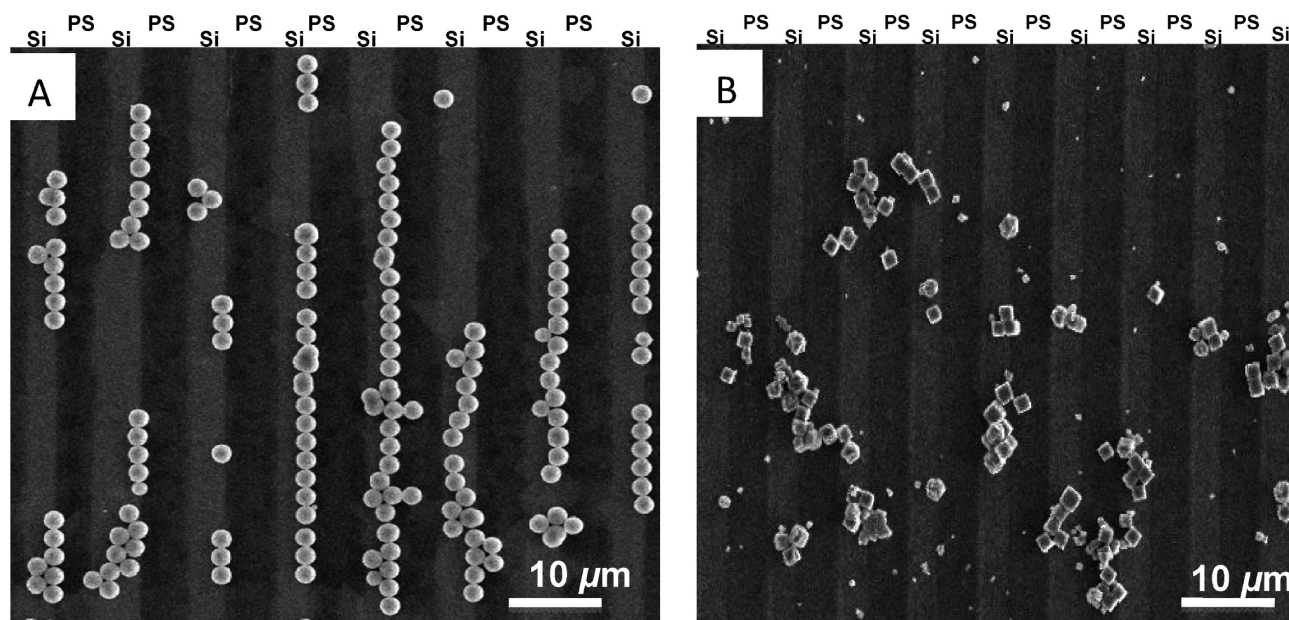


**Figure 6.** SEM images of the assembled spherical (A) and cubic (B) microparticles on the PS patterned silicon substrate (regions with PS and silicon are indicated).

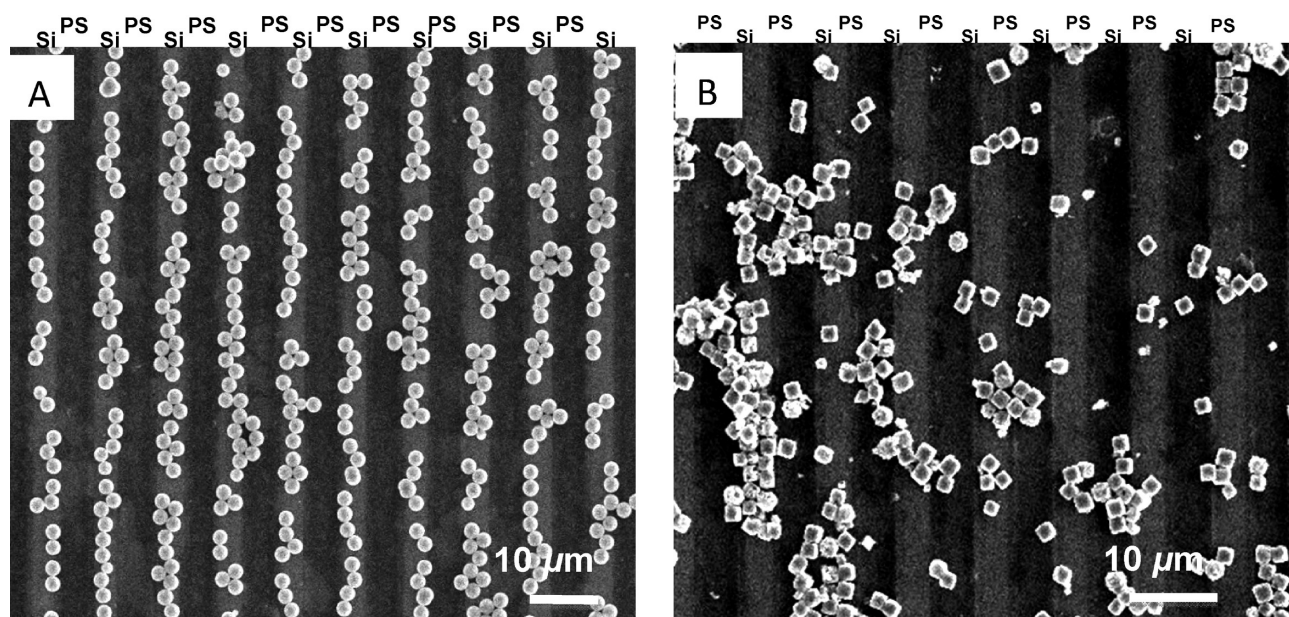


**Figure 7.** SEM images of the assembled spherical (A) and cubic (B) microparticles on the patterned silicon substrate functionalized with positively charged (PAH/PSS)<sub>3</sub>PAH coating.

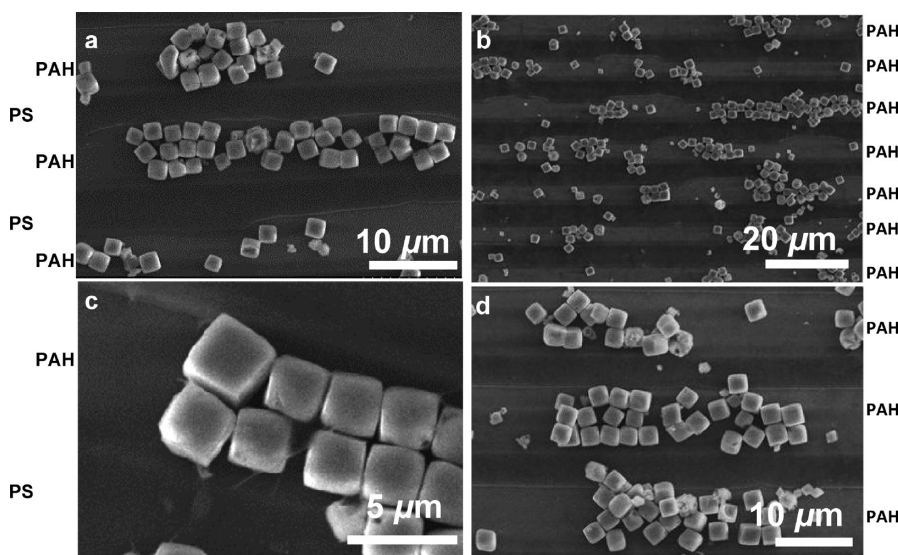


**Figure 8.** SEM images of the assemblies of functionalized cubic microparticles on the patterned silicon substrate functionalized with positively charged (PAH/PSS)<sub>3</sub>PAH coating.

odds of the spherical microparticles arranged in channels increased slightly to 98% with only very few microparticles found outside channels. For the cubic microparticles, the odds of their selective adsorption in channels also increased significantly and reached 70%, but this value still stays well below that observed for spherical microparticles (Figure 7).

In order to further improve the binding interaction between the cubic microparticles and functionalized patterned substrates with positively charged regions, the negatively charged LbL shell was assembled on the initial cores (Figure 1). Modification of cubic microparticles resulted in much increased negative surface potential (Table 1). For this combination, the much increased chance of predominant location of the cubic microparticles within the functionalized channels was observed with probability as high as 86% (Figure 8). Such a selectivity of cubic microparticles adsorption is much higher than that

observed for bare cubic microparticles and is comparable with that of regular spherical microparticles (Figure 9).

The balance of different forces acting on microparticles during deposition and assembly on patterned substrates depicted in Figure 4 should be evaluated in order to understand the underlying causes for these trends. We evaluated the electrostatic, capillary and Coulombic interactions of the bare and functionalized microparticles of different shapes with the patterned template used in this study (Figures 4 and 5). As known, the interfacial free energy of per unit contact area  $\Delta G^{\text{ad}}$  can be evaluated as a combination of surface free energies in accordance with the Dupre equation:<sup>49,50</sup>

$$\Delta G_{132}^{\text{ad}} = \gamma_{12} - \gamma_{13} - \gamma_{23} \quad (1)$$

where  $\gamma_{ij}$  is the interfacial free energy per unit area between phase  $i$  and  $j$  (Figure 10). The energy components of the two

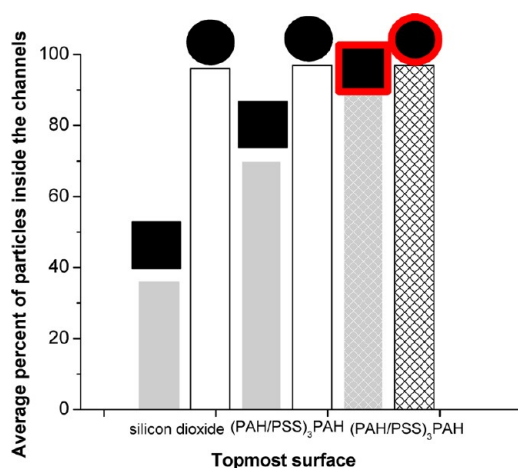


**Figure 9.** Average percent of the spherical (empty columns) and cubic (filled columns) microparticles and same microparticles coated with (PAH/PSS)<sub>2</sub> shells (crosshatched empty columns) on different substrates.

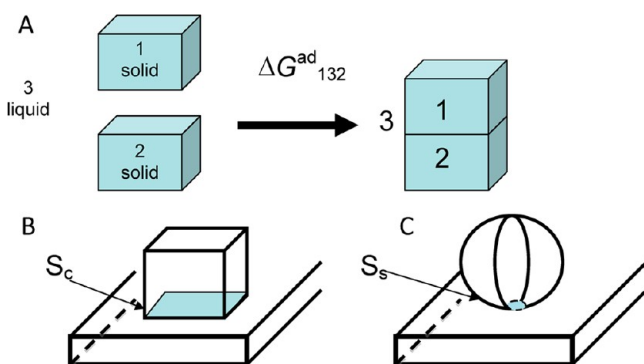


**Figure 10.** Interactions of the cubic microparticles (solid 1) with the substrate (solid 2) in water (liquid 3) (A). The contact surface areas of the cubic (B) and spherical (C) microparticles on the flat substrate.

surfaces in the aqueous dispersion can be calculated in accordance with usual approximation:<sup>51</sup>

$$\gamma_{ij} = \gamma_i + \gamma_j - 2\sqrt{\gamma_i^{LW}\gamma_j^{LW}} - 2\sqrt{\gamma_i^+\gamma_j^-} - 2\sqrt{\gamma_i^-\gamma_j^+} \quad (2)$$

where  $\gamma^{LW}$  is the van der Waals component,  $\gamma^-$  is the acidic component, and  $\gamma^+$  is the basic component.

In order to estimate the interaction energy for the microparticles due to immersion capillary forces,  $\Delta W^c$ , which arises from the deformation of the contact line at solid surface of microparticles in close proximity to the channel (Figure 11), we use the equation<sup>52,53</sup>

$$\Delta W^c(L) = -2\pi\gamma r_c \sin \Psi_{\infty} [h_c(L) - h_{\infty}] \quad (3)$$

where  $h_{\infty} = \gamma r_c \sin \Psi_{\infty} \ln(2/(\gamma_e q r_c))$ ,  $r_c$  is radius of the contact line,  $L$  is separation distance between the two microparticles,  $\Psi_{\infty}$  is the contact angle of the water with the particle's surface (which was taken to be equal to  $10^\circ$  for silica surfaces, as Nagayama et al. suggested<sup>50</sup>),  $h_c(L)$  represents the water's elevation above the planar liquid surface far from the microparticles, and  $h_{\infty}$  represents the water's elevation above the planar liquid surface infinitely far from the microparticles.  $\gamma_e = 1.781$  is a Euler–Masceroni constant, and  $q$  is the reverse capillary length (in the case of water  $q^{-1} = 2.7$  mm); other values used in these calculations are summarized in the

Supporting Information (Table S1). These equations could be applicable for both spherical and cubic microparticles with different radii of the contact line. The value  $r_c$  is constant for the cubic microparticles but changes with the height of the water layer for the spherical microparticles. Note that the flotation capillary force was not involved to the consideration because it is negligible with immersion and should be taken into account when the radius of the particles is larger than  $10 \mu\text{m}$ ,<sup>54</sup> whereas immersion can be significant even when radius is  $10$  nm.

In order to estimate the electrostatic interactions,  $\Delta V^e$ , between the particles and surface, we used the known linear superposition approximation<sup>16,55</sup>

$$\Delta V^e \approx \epsilon \Psi_{\text{par}} \Psi_{\text{temp}} \frac{R_1 R_2}{L} e^{-k(L-R_1-R_2)} \quad (4)$$

where  $\epsilon$  is the dielectric constant of the media,  $1/k$  is the characteristic Debye–Hückel length,  $R_1$  and  $R_2$  are the radii of the interacting microparticles,  $L$  is the distance between the interacting microparticles, and  $\Psi_{\text{par}}$  and  $\Psi_{\text{temp}}$  are the surface potentials of the particles and the template, respectively. To apply this model to our system, we assume that the template spacing ( $R_2 = 10 \mu\text{m}$ ) is much larger than microparticle dimensions ( $R_1 = 2.5 \mu\text{m}$ ).  $L = R_1 + R_2 + h$  is the distance between the template and particles for the smaller separation  $h \rightarrow 0$ . Zeta potential values were applied to the above equation as estimated earlier (Table 1).

The different interfacial energies evaluated from eqs 1–4 are summarized in Table 2. The analysis of these data shows that the interfacial forces for cubic microparticle–surface contacts are comparable to capillary forces exerted onto the cubic microparticles onto PS regions. In contrast, the interfacial energy for spherical microparticle–surface contacts is 4 orders of magnitude lower than the capillary energy. Meanwhile, the Coulombic interactions between the substrate and the microparticles are 4 orders of magnitude lower than the capillary forces for both spherical and cubic microparticles. Thus, the spherical microparticles can be easily dragged by the capillary forces into the channels despite the repulsive Coulombic interactions between the bare silicon substrate and silica microparticles ( $\Delta V_{\text{SiO}_2/\text{Si}_w} = +2.5 \times 10^{-18}$  J) and high adhesion of silica microparticles to PS regions ( $-\Delta W_{\text{SiO}_2/\text{PS}}^a > +\Delta W_{\text{SiO}_2/\text{PAH}}^a$ ) (Figure 6A and Table 2).

In contrast to spherical microparticles, the interfacial adhesion becomes a dominant factor in the assembly of the cubic microparticles. Indeed, the contact cubic microparticle–substrate area of  $6.25 \mu\text{m}^2$  (Figure 10B) is dramatically higher than that for the spherical microparticles with a minute contact area of  $625 \text{ nm}^2$  (Figure 10B) (as estimated from geometrical dimensions and light Hertzian deformation for spherical microparticles in contact with planar surface<sup>56</sup>). According to the statistical evaluation of the cubic microparticles on the PS regions with partial contacts, the average contact area can be estimated to be close  $4 \mu\text{m}^2$  per microparticle. The average adhesive energy of bare cubic microparticles does not differ significantly at different regions: the PS surface ( $\Delta W_{\text{PS}/\text{MnCO}_3}^a = 15 \times 10^{-14}$  J), bare substrate ( $\Delta W_{\text{Si}/\text{MnCO}_3}^a = 28.1 \times 10^{-14}$  J), or functionalized substrate ( $\Delta W_{\text{PAH}/\text{MnCO}_3}^a = 33.2 \times 10^{-14}$  J) (Table 2). Thus, the distribution of bare cubic microparticles stays relatively random with modest tendency to preferentially tether to functionalized channels.

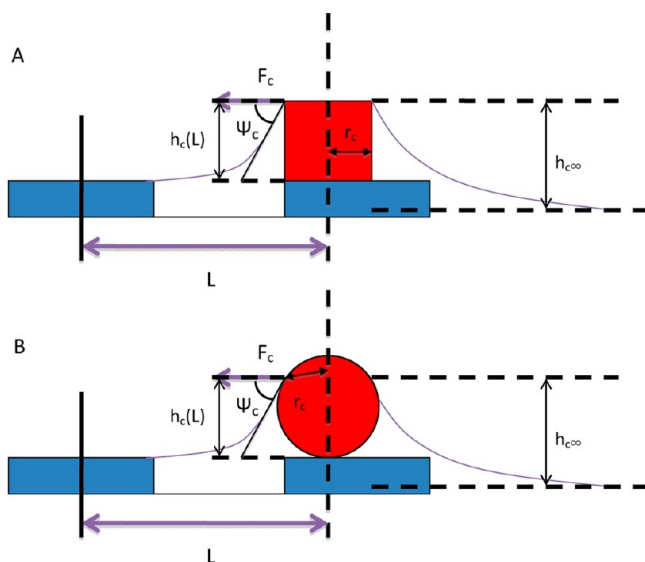


**Figure 11.** Capillary interaction of the cubic (A) and spherical (B) microparticles immersed in a liquid layer;  $r_c$  is radius of the contact line,  $L$  is separation distance between the two particles,  $\Psi_{\infty}$  is the contact angle of the water with the particle's surface,  $h_c(L)$  represents the water's elevation above the planar liquid surface far from the microparticles, and  $h_{\infty}$  represents the water's elevation above the liquid surface infinitely far from the microparticles.

The functionalization of the cubic microparticles with the negatively charged shells leads to the significant changes in the binding energy with functionalized channels from  $33.2 \times 10^{-14}$  to  $-10.5 \times 10^{-14}$  J (Table 2). Overall, total interaction energy ( $\Delta W^{\text{tot}}$ ) between the functionalized substrate and the functionalized cubic microparticles allows to overcome the  $\Delta W^{\text{tot}}$  between the cubic microparticles and PS regions and drive them into the channels by the receding front. Therefore, we can conclude that only a combination of high repulsion outside of channels and high adhesion inside channels may lead to selective assembly of cubic microparticles inside channels and the formation of chain-like aggregates of cubes. This behavior is in a contrast to assembling of traditional spherical microparticles which are dragged inside channels by strong capillary forces disregarding minute details and differences of interfacial interactions in very small contact areas. The consideration geometry of the PS pattern (width and bending) on the final assemblies may be an interesting subject of further studies.

Our results should be also considered in lieu of recent studies of colloidal assemblies on patterned substrates with general

understanding that the directed assembly of the spherical microparticles can be easily controlled through the capillary forces and Coulombic interactions with some role of entropic factors and interparticle interactions noted.<sup>57,58</sup> In fact, the control of the adhesive forces of the cuboid silica microparticles was reported by Onoe et al.<sup>59</sup> By utilizing different self-assembly monolayers, the authors achieved the preferable binding pattern in the case of dramatic reduction of the capillary forces (exchanging water with isopropanol and by heating to 110 °C). According to another study from the same group, the adhesion forces become significant at a certain aspect ratio of the base to the height.<sup>60</sup> Hammond et al. demonstrated the control of the selective assembly of the spherical silica nanoparticles (100–500 nm in diameter) by coating patterned templates with LbL coatings with dominated of Coulombic interactions. In another study, Schweikart et al.<sup>19</sup> controlled the assembly of spherical microparticles by capillary forces within wrinkle patterns. Experimental studies and numerical analysis of the cylindrical microparticles demonstrated that the assembly with preferred orientation can be achieved.<sup>61,62</sup> On the basis of Stebe's group the shape anisotropy creates undulations with excess area that locally elevates at certain locations around the particle, and therefore excess energy makes these particles to orient and aggregate in preferred orientations. The effect of the shapes on the colloidal assembly was also reported by Lapointe et al.<sup>63</sup> Liu et al. assembled the zirconate titanate microcrystal (PZT) with cubic shape (2–3  $\mu\text{m}$  in size) into a densely packed monolayer by utilizing a Langmuir–Blodgett monolayers.<sup>64</sup> A uniformly oriented array of cubic microparticles has been produced via balance of the spreading tension, surface tension, interfacial tension, wetting forces, and capillary forces.

In conclusion, we considered the pattern-assisted assembly of spherical and cubic microparticles with the controlled interfacial forces. The difference in assembling behavior of cubic (random) and spherical (selective) microparticles was related to the fact that the adhesive forces between the cubic microparticles and the substrate are 4 orders of magnitude higher than that for the spherical microparticles due to the significantly higher contact area of cubic microparticles on flat surfaces. Therefore, the probability of the spherical microparticles assembling in the channels is significantly higher due to the low adhering of microparticles and overall domination of capillary forces. However, a highly selective assembly of cubic microparticles inside channels can be achieved via the chemical modification of cubic microparticles as well as patterned substrates, which can be suggested as a convenient route to

**Table 2.** Adhesion  $\Delta W^{\text{a}}$ , Capillary,  $\Delta W^{\text{c}}$ , Electrostatic,  $\Delta V^{\text{e}}$ , and Total,  $\Delta W^{\text{tot}}$ , Interfacial Energies between the Bare/Modified Microparticles and the Bare/Modified Substrates

surfaces	$\Delta G^{\text{ad}}$ (mJ/m <sup>2</sup> )	$\Delta W^{\text{a}}$ (J)	$\Delta W^{\text{c}}$ (J)	$\Delta V^{\text{e}}$ (J)	$\Delta W^{\text{tot}}$ (J)
PS/(MnCO <sub>3</sub> )PSS	-45.6	$-18 \times 10^{-14}$	$-9.6 \times 10^{-14}$	neutral	$-8.4 \times 10^{-14}$
PAH/(MnCO <sub>3</sub> )PSS	-16.95	$-10.5 \times 10^{-14}$		$-2 \times 10^{-18}$	$-10.5 \times 10^{-14}$
PS/MnCO <sub>3</sub>	36.11	$15 \times 10^{-14}$	$-9.6 \times 10^{-14}$	neutral	$5.4 \times 10^{-14}$
PAH/MnCO <sub>3</sub>	53.19	$33.2 \times 10^{-14}$		$-1.3 \times 10^{-18}$	$33.2 \times 10^{-14}$
Si_wafer/MnCO <sub>3</sub>	44.9	$28.1 \times 10^{-14}$		$+1 \times 10^{-18}$	$28.1 \times 10^{-14}$
Si_wafer/SiO <sub>2</sub>	-2	$-1.3 \times 10^{-18}$		$+2.5 \times 10^{-18}$	$-1.3 \times 10^{-18}$
PS/SiO <sub>2</sub>	-7	$-4.7 \times 10^{-18}$	$-9.6 \times 10^{-14}$	neutral	$-9.6 \times 10^{-14}$
PAH/SiO <sub>2</sub>	21	$13 \times 10^{-18}$		$-3 \times 10^{-18}$	$10 \times 10^{-18}$
PAH/(SiO <sub>2</sub> )PSS	-16.95	$-10.5 \times 10^{-18}$		$-3 \times 10^{-18}$	$-13.5 \times 10^{-18}$
PS/(SiO <sub>2</sub> )PSS	-45.6	$-28.5 \times 10^{-18}$	$-9.6 \times 10^{-14}$	neutral	$-9.6 \times 10^{-14}$

direct the colloidal assembly of cubic microparticles into ordered arrays. The ability to control the selective deposition anisotropic microparticles by functionalizing LbL coating is critically important for the design biosensing devices.<sup>36</sup>

## ■ ASSOCIATED CONTENT

### ● Supporting Information

Table 1S and SEM images of the guided assembly. This material is available free of charge via the Internet at <http://pubs.acs.org>.

## ■ AUTHOR INFORMATION

### Corresponding Author

\*E-mail: [Vladimir@mse.gatech.edu](mailto:Vladimir@mse.gatech.edu).

### Notes

The authors declare no competing financial interest.

## ■ ACKNOWLEDGMENTS

This work was supported by the U.S. Department of Energy, Office of Basic Energy Sciences, Division of Materials Sciences and Engineering, under Award # DE-FG02-09ER46604.

## ■ REFERENCES

- (1) Glotzer, S. C.; Solomon, M. L. Anisotropy of building blocks and their assembly into complex structures. *Nat. Mater.* **2007**, *6*, 557–562.
- (2) Ruiz-Hitzky, E.; Darder, M.; Aranda, P.; Ariga, K. Advances in biomimetic and nanostructured biohybrid materials. *Adv. Mater.* **2010**, *22*, 323–336.
- (3) Tsukruk, V. V. Assembly of supramolecular polymers in ultrathin films. *Prog. Polym. Sci.* **1997**, *22*, 247–311.
- (4) Cohen-Stuart, M. C.; Huck, W.; Genzer, J.; Muller, M.; Ober, C.; Stamm, M.; Sukhorukov, G.; Szleifer, I.; Tsukruk, V. V.; Urban, M.; Winnik, F.; Zauscher, S.; Luzinov, I.; Minko, S. Emerging applications of stimuli-responsive polymer materials. *Nat. Mater.* **2010**, *9*, 101–113.
- (5) Fakhruddin, R. F.; Lvov, Y. M. “Face-lifting” and “make-up” for microorganisms: layer-by-layer polyelectrolyte nanocoating. *ACS Nano* **2012**, *6*, 4557–4564.
- (6) García-Alonso, J.; Fakhruddin, R. F.; Paunov, V.N.; Shen, Z.; Hardege, J. D.; Pamme, N.; Haswell, S. J.; Greenway, G. M. Microscreening toxicity system based on living magnetic yeast and gradient chips. *Anal. Bioanal. Chem.* **2011**, *400*, 1009–1013.
- (7) Mirkin, C. A. Programming the assembly of 2 and 3D architectures with DNA and nanoscale inorganic building blocks. *Inorg. Chem.* **2000**, *39*, 2258–2272.
- (8) Davis, S. A.; Breulmann, M.; Rhodes, K. H.; Zhang, B.; Mann, S. Template-directed assembly using nanoparticle building blocks: A nanotectonic approach to organized materials. *Chem. Mater.* **2001**, *13*, 3218–3226.
- (9) Xia, D.; Biswas, A.; Li, D.; Brueck, S. Directed self-assembly of silica nanoparticles into nanometer-scale patterned surfaces using spin-coating. *Adv. Mater.* **2004**, *16*, 1427–1432.
- (10) Fudouzi, H.; Kobayashi, M.; Shinya, N. Assembling 100 nm scale particles by an electrostatic potential field. *J. Nanopart. Res.* **2001**, *3*, 193–200.
- (11) Zhao, Q.; Fan, T.; Ding, J.; Zhang, D.; Guo, Q.; Kamada, M. Super black and ultrathin amorphous carbon film inspired by anti-reflection architecture in butterfly wing. *Carbon* **2011**, *49*, 877–883.
- (12) Han, K. S.; Shin, J. H.; Yoon, W. Y.; Lee, H. Enhanced performance of solar cells with anti-reflection layer fabricated by nano-imprint lithography. *Sol. Energy Mater. Sol. Cells* **2011**, *95*, 288–291.
- (13) Chen, J. Y.; Chang, W. I.; Huang, C. K.; Sun, K. W. Biomimetic nanostructured antireflection coating and its application on crystalline silicon solar cells. *Opt. Express* **2011**, *19*, 14411–14419.
- (14) Cai, J.; Ye, J.; Chen, S.; Zhao, X.; Zhang, D.; Chen, S.; Ma, Y.; Jin, S.; Qi, L. Self-cleaning, broadband and quasi-omnidirectional

antireflective structures based on mesocrystalline rutile TiO<sub>2</sub> nanorod arrays. *Energy Environ. Sci.* **2012**, *5*, 7575–7581.

- (15) Liu, H.; Zhao, Q.; Zhou, H.; Ding, J.; Zhang, D.; Zhu, H.; Fan, T. Hydrogen evolution via sunlight water splitting on an artificial butterfly wing architecture. *Phys. Chem. Chem. Phys.* **2011**, *13*, 10872–10876.

- (16) Kim, Y. H.; Park, J.; Hammond, P. T. Selective assembly of colloidal particles on a nanostructured template coated with polyelectrolyte multilayers. *Adv. Mater.* **2007**, *19*, 4426–4430.

- (17) van Blaaderen, A.; Ruel, R.; Wiltzius, P. Template-directed colloidal crystallization. *Nature* **1997**, *385*, 321–324.

- (18) Lopes, W. A.; Jaeger, H. M. Hierarchical self-assembly of metal nanostructures on diblock copolymer scaffolds. *Nature* **2001**, *414*, 735–738.

- (19) Schewikart, A.; Pazos-Perez, N.; Alvarez-Puebla, A. R.; Fery, A. Controlling inter-nanoparticle coupling by wrinkle-assisted assembly. *Soft Matter* **2011**, *7*, 4093–4100.

- (20) Kim, J.-W.; Fernandez-Nieves, A.; Dan, N.; Utada, A. S.; Marquez, M.; Weitz, D. A. Colloidal assembly route for responsive colloidosomes with tunable permeability. *Nano Lett.* **2007**, *7*, 2876–2880.

- (21) Han, L.; Maye, M. M.; Leibowitz, F. L.; Ly, N. K.; Zhong, C. J. Quartz-crystal microbalance and spectrophotometric assessments of inter-core and inter-shell reactivities in nanoparticle thin film formation and growth. *J. Mater. Chem.* **2001**, *11*, 1258–1264.

- (22) Hirakata, H.; Ajioka, Y.; Yonezu, A.; Minoshima, K. Fabrication and mechanical properties of column-particle nanocomposites by multiscale shape-assisted self-assembly. *J. Phys. D.: Appl. Phys.* **2012**, *45*, 0253021–0253028.

- (23) Stauth, S. A.; Parviz, B. A. Self-assembled single-crystal silicon circuits on plastic. *Proc. Natl. Acad. Sci. U. S. A.* **2006**, *103*, 13922–13927.

- (24) Ahnizay, A.; Sakamoto, Y.; Bergstrom, L. Magnetic field-induced assembly of oriented superlattices from maghemite nanocubes. *Proc. Natl. Acad. Sci. U. S. A.* **2007**, *104*, 17570–17574.

- (25) Jiang, C.; Markutsya, S.; Shulha, H.; Tsukruk, V. V. Freely suspended gold nanoparticles arrays. *Adv. Mater.* **2005**, *17*, 1669–1673.

- (26) Jiang, C.; Singamaneni, S.; Merrick, E.; Tsukruk, V. V. Complex buckling instability patterns of nanomembranes with encapsulated gold nanoparticle arrays. *Nano Lett.* **2006**, *6*, 2254–2259.

- (27) Shchepelina, O.; Kozlovskaya, V.; Singamaneni, S.; Kharlampieva, E.; Tsukruk, V. V. Replication of anisotropic dispersed particulates and complex continuous templates. *J. Mater. Chem.* **2010**, *20*, 6587–6603.

- (28) Rolland, J. P.; Maynor, B. W.; Euliss, L. E.; Exner, A. E.; Denison, G. M.; DeSimone, J. M. Direct fabrication and harvesting of monodisperse, shape specific nano-biomaterials. *J. Am. Chem. Soc.* **2005**, *127*, 10096–10100.

- (29) Jones, M. R.; Macfarlane, R. J.; Lee, B.; Zhang, J.; Young, K. L.; Senesi, A. J.; Mirkin, C. A. DNA-nanoparticle superlattices formed from anisotropic building blocks. *Nat. Mater.* **2010**, *9*, 913–917.

- (30) Rycenga, M.; McLellan, J. M.; Xia, Y. Controlling the assembly of silver nanocubes through selective functionalization of their faces. *Adv. Mater.* **2008**, *20*, 2416–2420.

- (31) Tang, Z.; Zhang, Z.; Wang, Y.; Glotzer, S. C.; Kotov, N. A. Self-assembly of CdTe nanocrystals into free-floating sheets. *Science* **2006**, *314*, 274–278.

- (32) Chen, Q.; Whitmer, J. K.; Jiang, S.; Bae, S. C.; Luijten, E.; Granick, S. Supracolloidal reaction kinetics of Janus spheres. *Science* **2011**, *131*, 199–202.

- (33) Chen, Q.; Bae, S. C.; Granick, S. Directed self-assembly of a colloidal kagome lattice. *Nature* **2011**, *469*, 381–384.

- (34) Gao, B.; Arya, G.; Tao, A. R. Self-orienting nanocubes for the assembly of plasmonic nanojunctions. *Nature Nanotechnol.* **2012**, DOI: 10.1038/NNANO.2012.83.

- (35) Caruso, F. *Colloids and Colloid Assemblies: Synthesis, Modification, Organization and Utilization of Colloid Particles*; Wiley-VCH: Weinheim, 2004.

- (36) Drachuk, I.; Shchepelina, O.; Lisunova, M.; Harbaugh, S.; Kelley-Loughnane, N.; Stone, M.; Tsukruk, V. V. pH-Responsive LbL nanoshells for direct regulation of cell activity. *ACS Nano* **2012**, *6*, 4266–4278.
- (37) Zhu, H.; Stein, E. W.; Lu, Z.; Lvov, Y. M.; McShane, M. J. Synthesis of size-controlled monodisperse manganese carbonate microparticles as templates for uniform polyelectrolyte microcapsule form. *Chem. Mater.* **2005**, *17*, 2323–2328.
- (38) Kozlovskaya, V.; Kharlampieva, E.; Khanal, B. P.; Manna, P.; Zubarev, E. R.; Tsukruk, V. V. Ultrathin layer-by-layer hydrogels with incorporated gold nanorods as pH-sensitive optical materials. *Chem. Mater.* **2008**, *20*, 7474–7485.
- (39) Ko, H.; Jiang, C.; Tsukruk, V. V. Encapsulating nanoparticle arrays into layer-by-layer multilayers by capillary transfer lithography. *Chem. Mater.* **2005**, *17*, 5489–549.
- (40) Kharlampieva, E.; Kozlovskaya, V.; Chan, J.; Ankner, J. F.; Tsukruk, V. V. Spin-assisted layer-by-layer assembly: variation of stratification as studied with neutron reflectivity. *Langmuir* **2009**, *25*, 14017–14024.
- (41) Jiang, C.; Markutsya, S.; Pikus, Y.; Tsukruk, V. V. Freely suspended nanocomposite membranes as highly-sensitive sensors. *Nat. Mater.* **2004**, *3*, 721–728.
- (42) Jiang, C.; Markutsya, S.; Tsukruk, V. V. Compliant, robust, and truly nanoscale free-standing multilayer films fabricated using spin-assisted layer-by-layer assembly. *Adv. Mater.* **2004**, *16*, 157–161.
- (43) Tsukruk, V. V.; Bliznyuk, V. N. Adhesive and friction forces between chemically modified silicon and silicon nitride surfaces. *Langmuir* **1998**, *14*, 446–455.
- (44) Tsukruk, V. V.; Reneker, D. H. Scanning probe microscopy of polymeric and organic molecular films: from self-assembled monolayers to composite multilayers. *Polymer* **1995**, *36*, 1791–1808.
- (45) McConney, M. E.; Singamaneni, S.; Tsukruk, V. V. Probing soft matter with the Atomic Force Microscope: force-spectroscopy and beyond. *Polym. Rev.* **2010**, *50*, 235–286.
- (46) Tsukruk, V. V.; Huang, Z.; Chizhik, S. A.; Gorbunov, V. V. Probing of micromechanical properties of compliant polymeric materials. *J. Mater. Sci.* **1998**, *33*, 4905–4909.
- (47) Shchepelina, O.; Kozlovskaya, V.; Kharlampieva, E.; Mao, W.; Alexeev, A.; Tsukruk, V. V. Anisotropic micro- and nano-capsules. *Macromol. Rapid Commun.* **2010**, *31*, 2041–2046.
- (48) Kozlovskaya, V.; Kharlampieva, E.; Drachuk, I.; Cheng, D.; Tsukruk, V. V. Responsive microcapsule reactors based on hydrogen-bonded tannic acid layer-by-layer assemblies. *Soft Matter* **2010**, *6*, 3596–3608.
- (49) van Oss, C. J.; Good, R. J.; Chaudhury, M. K. The role of van der Waals force and hydrogen bonds in “Hydrophobic interactions” between biopolymers and low energy surfaces. *J. Colloid Interface Sci.* **1986**, *111*, 378–390.
- (50) van Oss, C. J.; Good, R. J.; Chaudhury, M. K. Additive and nonadditive surface tension components and the interpretation of contact angles. *Langmuir* **1988**, *4*, 884–891.
- (51) Girifalco, L. A.; Good, R. J. A theory for the estimation of surface and interfacial energies. I. derivation and application to interfacial tension. *J. Phys. Chem.* **1957**, *61*, 904–909.
- (52) Kralchevsky, P. A.; Nagayama, K. Capillary forces between colloidal particles. *Langmuir* **1994**, *10*, 23–36.
- (53) Kralchevsky, P. A.; Paunov, V. N.; Inanov, I. B.; Nagayama, K. Capillary meniscus interactions between colloidal particles attached to a liquid-fluid interface. *J. Colloid Interface Sci.* **1992**, *151*, 79–94.
- (54) Kralchevsky, P. A.; Denkov, N. D.; Paunov, V. N.; Veleev, O. D.; Inanov, I. B.; Yoshimura, H.; Nagayama, K. Formation of two-dimensional colloid crystals in liquid films under the action of capillary forces. *J. Phys.: Condens. Matter* **1994**, *6*, A395–A402.
- (55) Aizenberg, J.; Braun, P. V.; Wiltzius, P. Patterned colloidal deposition controlled by electrostatic and capillary forces. *Phys. Rev. Lett.* **2000**, *84*, 2997–3000.
- (56) Tsukruk, V. V.; Singamaneni, S. *Scanning Probe Microscopy of Soft Matter: Fundamentals and Practices*; Wiley-VCH: Weinheim, 2012.
- (57) Onsager, L. The effects of shape on the interaction of colloidal particles. *Ann. N.Y. Acad. Sci.* **1949**, *51*, 627–659.
- (58) Ming, T.; Kou, X.; Chen, H.; Wang, T.; Tam, H.; Cheah, K.; Chen, J.; Wang, J. Ordered gold nanostructure assemblies formed by droplet evaporation. *Angew. Chem., Int. Ed.* **2008**, *47*, 9685–9690.
- (59) Onoe, H.; Matsumoto, K.; Shimoyama, I. Three-dimensional micro-self-assembly using hydrophobic interaction controlled by self-assembled monolayers. *J. Microelectromech. Syst.* **2004**, *13*, 603–611.
- (60) Onoe, H.; Gel, M.; Hoshino, K.; Matsumoto, K.; Shimoyama, I. Direct measurement of the binding force between microfabricated particles and a planar surface in aqueous solution by force-sensing piezoresistive cantilevers. *Langmuir* **2005**, *21*, 11251–11261.
- (61) Lewandowski, E.; Bernate, J.; Tseng, A.; Searson, P.; Stebe, K. Oriented assembly of anisotropic particles by capillary interactions. *Soft Matter* **2009**, *5*, 886–890.
- (62) Lewandowski, E.; Cavallaro, M.; Botto, L.; Bernate, J.; Garbin, V.; Stebe, K. Orientation and self-assembly of cylindrical particles by anisotropic capillary interactions. *Langmuir* **2010**, *26* (19), 15142–15154.
- (63) Lapointe, C. P.; Mason, T. G.; Smalyukh, I. I. Shape-controlled colloidal interactions in nematic liquid crystals. *Science* **2009**, *326*, 1083–1086.
- (64) Liu, X.; McCandlish, E. F.; McCandlish, L. E.; Mikulka-Bolen, K.; Ramesh, R.; Cosandey, F.; Rossetti, G. A.; Riman, R. E. Single-crystal-like materials by the self-assembly of cube-shaped lead zirconate titanate (PZT) microcrystals. *Langmuir* **2005**, *21*, 3207–3212.
- (65) Reihls, T.; Muller, M.; Lunkwitz, K. Deposition of polyelectrolyte complex nano-particles at silica surfaces characterized by ATR-FTIR and SEM. *Colloids Surf., A* **2003**, *212*, 79–95.